

Deformation-Free Cross-Domain Image Registration via Position-Encoded Temporal Attention

Yiwen Wang and Jiahao Qin*

Abstract. We address the problem of cross-domain image registration, where paired images I_m and I_f exhibit coupled geometric misalignment and domain-specific appearance shift. We formalize this as a factorization problem: decomposing each image into a domain-invariant scene representation $\mathbf{s} \in \mathbb{R}^{C \times H \times W}$ and a global appearance statistic $\mathbf{a} \in \mathbb{R}^d$, such that registration reduces to recombining the scene structure of I_m with the appearance of I_f via Adaptive Instance Normalization (AdaIN). This factorization eliminates the need for explicit deformation field estimation. To exploit temporal coherence in sequential acquisitions, we introduce a position-encoded cross-frame attention mechanism that fuses learnable and sinusoidal position embeddings with multi-head attention over a sliding window of k neighboring frames, enriching the scene representation with inter-frame context. We instantiate this framework as GPEReg-Net and evaluate on two benchmarks: FIRE-Reg-256 (retinal fundus, semi-rigid) and HPatches-Reg-256 (synthetic textured patches, affine). GPEReg-Net achieves state-of-the-art performance on both benchmarks (FIRE: SSIM = 0.928, PSNR = 33.47 dB; HPatches: SSIM = 0.450, PSNR = 21.01 dB), surpassing all baselines including deformation-based methods, while running $1.87\times$ faster than SAS-Net. Code: <https://github.com/JiahaoQin/GPEReg-Net>.

Keywords: Image registration · Scene-appearance factorization · Deformation-free alignment · Position-encoded attention · Cross-domain generalization

1 Introduction

Let $I_m, I_f \in \mathbb{R}^{H \times W}$ denote a moving image and a fixed image, respectively. Image registration seeks a mapping $\mathcal{T} : I_m \mapsto \hat{I}_r$ such that $\hat{I}_r \approx I_f$ under a suitable similarity measure [25, 5]. In cross-domain settings—where I_m and I_f are drawn from different intensity distributions due to varying acquisition conditions (e.g., subject motion in retinal imaging [8], viewpoint changes in natural images [3])—the brightness constancy assumption $I_m(\mathbf{x}) \approx I_f(\mathbf{x} + \mathbf{u})$ underlying conventional methods [5] is systematically violated.

Limitations of existing approaches. Classical methods—SIFT [12], Demons [27], optical flow [9], SyN [1]—estimate spatial correspondences directly but degrade when intensity distributions differ. Learned deformation

* Corresponding author: jiahao.qin19@gmail.com

methods (VoxelMorph [2], TransMorph [4], spatial transformer networks [11], Laplacian pyramid approaches [13]) parameterize \mathcal{T} as a displacement field $\mathbf{u}(\mathbf{x})$ but inherit the same intensity assumption. Scene-appearance separation frameworks [23,21] address domain shift through disentangled latent spaces but employ complex generative architectures without temporal awareness. Progressive strategies [22] improve alignment iteratively but do not explicitly factorize appearance from scene content.

Key insight. We observe that the cross-domain registration problem admits a natural *factorization*: each image can be decomposed into a domain-invariant scene representation \mathbf{s} (encoding spatial structure) and a domain-specific appearance statistic \mathbf{a} (encoding intensity profile). Registration then reduces to recombining \mathbf{s}_m with \mathbf{a}_f via Adaptive Instance Normalization (AdaIN) [10], yielding $\hat{I}_r = \mathcal{D}(\text{AdaIN}(\mathbf{s}_m, \mathbf{a}_f))$ without estimating any deformation field [14,16,18]. Furthermore, in sequential acquisitions, temporal coherence between consecutive frames can be exploited via position-encoded cross-frame attention [26,17,15] to improve inter-frame consistency.

We instantiate this insight as **GPEReg-Net** and make the following contributions:

1. **Scene-appearance factorization.** We formalize cross-domain registration as a latent factorization problem and propose an encoder-decoder architecture that decomposes images into domain-invariant scene features $\mathbf{s} \in \mathbb{R}^{64 \times H \times W}$ and global appearance codes $\mathbf{a} \in \mathbb{R}^{32}$, with AdaIN-based recombination that eliminates deformation field estimation entirely.
2. **Position-encoded temporal attention.** We introduce a Global Position Encoding (GPE) module that fuses learnable position embeddings, sinusoidal encoding, and multi-head cross-frame attention over a sliding window of k neighbors, enabling the model to exploit temporal structure in sequential acquisitions.
3. **Comprehensive cross-domain evaluation.** We validate on two diverse benchmarks—FIRE-Reg-256 (retinal fundus, semi-rigid) and HPatches-Reg-256 (synthetic patches, affine)—achieving state-of-the-art results on both while maintaining real-time throughput (69 FPS).

2 Proposed Method: GPEReg-Net

2.1 Problem Formulation and Architecture Overview

Given a moving image $I_m \in \mathbb{R}^{H \times W}$ and a fixed image $I_f \in \mathbb{R}^{H \times W}$ drawn from potentially different intensity distributions, our goal is to learn a mapping $\mathcal{T}_\theta : (I_m, I_f) \mapsto \hat{I}_r$ such that \hat{I}_r is geometrically aligned with I_f while adopting its intensity profile, *without* estimating an explicit deformation field $\mathbf{u} : \mathbb{R}^2 \rightarrow \mathbb{R}^2$.

We decompose \mathcal{T}_θ into four learned modules (fig. 1):

1. **SceneEncoder \mathcal{S} :** Extracts domain-invariant scene features $\mathbf{s} = \mathcal{S}(I_m)$ via instance normalization, discarding appearance information.

2. **AppearanceEncoder** \mathcal{A} : Extracts a global appearance code $\mathbf{a} = \mathcal{A}(I_f)$ that captures the intensity profile of the target domain.
3. **Global Position Encoding** \mathcal{G} : Enhances scene features with temporal context: $\tilde{\mathbf{s}} = \mathcal{G}(\mathbf{s}, t)$, where t is the frame index.
4. **ImageDecoder** \mathcal{D} : Reconstructs the registered output using AdaIN modulation: $\hat{I}_r = \mathcal{D}(\tilde{\mathbf{s}}, \mathbf{a})$.

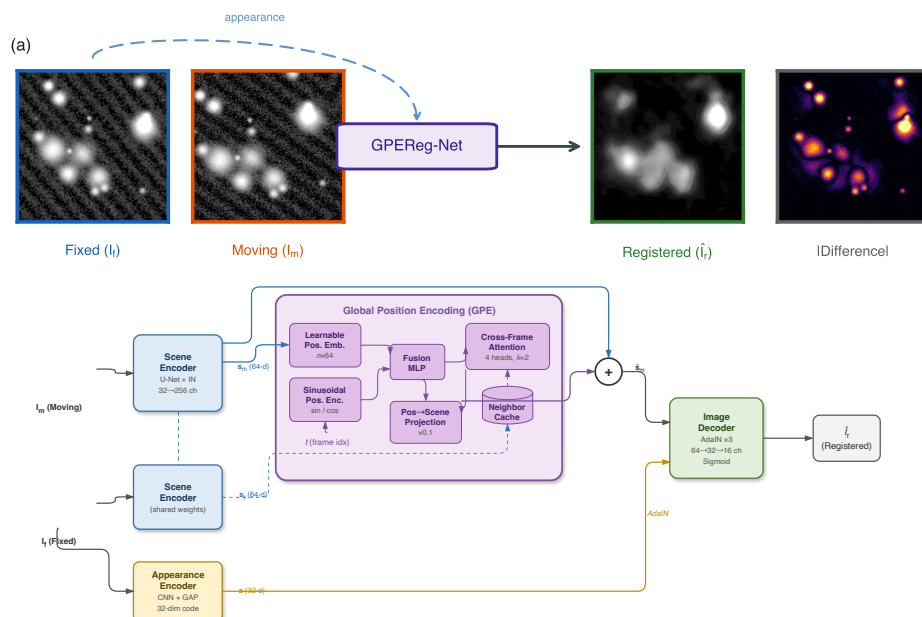


Fig. 1. (a) Registration example on HPatches-Reg-256 [3]: the fixed image I_f , moving image I_m with geometric misalignment, the registered output \hat{I}_r produced by GPEReg-Net, and the absolute difference $|I_r - I_f|$. A dashed arrow indicates the appearance pathway from I_f . (b) Overview of GPEReg-Net. The SceneEncoder \mathcal{S} extracts domain-invariant features \mathbf{s} from the moving image I_m using instance normalization. The AppearanceEncoder \mathcal{A} extracts a 32-dim global appearance code \mathbf{a} from the fixed image I_f . The GPE module \mathcal{G} enriches scene features with temporal context via learnable position embeddings, sinusoidal encoding, and cross-frame attention, producing $\tilde{\mathbf{s}}$. The ImageDecoder \mathcal{D} uses AdaIN to modulate enhanced scene features with the target appearance, producing the registered output \hat{I}_r without any explicit deformation field.

2.2 Scene-Appearance Factorization via Dual Encoders

The **SceneEncoder** extracts domain-invariant features from the moving image using a U-Net [24] backbone with residual connections [7] and Instance Normalization (IN), which strips per-instance intensity statistics while preserving

spatial structure. It produces a 64-dimensional scene feature map $\mathbf{s} \in \mathbb{R}^{64 \times H \times W}$ via four encoding levels ($C_l \in \{32, 64, 128, 256\}$) with bilinear upsampling decoder and skip connections.

The **AppearanceEncoder** extracts a 32-dimensional global appearance code $\mathbf{a} \in \mathbb{R}^{32}$ from the fixed image via four stride-2 convolutions, Global Average Pooling, and two FC layers, capturing target domain intensity statistics without spatial information.

The **ImageDecoder** reconstructs the registered output by injecting the target appearance into scene features using Adaptive Instance Normalization (AdaIN) [10]:

$$\text{AdaIN}(\mathbf{s}, \mathbf{a}) = \gamma(\mathbf{a}) \cdot \frac{\mathbf{s} - \mu(\mathbf{s})}{\sigma(\mathbf{s})} + \beta(\mathbf{a}), \quad (1)$$

where $\gamma(\mathbf{a})$ and $\beta(\mathbf{a})$ are learned affine parameters. Three AdaIN-Conv blocks (64, 32, 16 channels) progressively reconstruct the output \hat{I}_r without any spatial deformation field.

2.3 Position-Encoded Cross-Frame Temporal Attention

The GPE module exploits temporal structure in sequential acquisitions by enriching scene features with inter-frame positional context before decoding. For frame index $t \in \{0, \dots, N-1\}$, the module computes a position-aware representation by combining: (1) a *learnable position embedding* $\mathbf{e}_t \in \mathbb{R}^{64}$ from an embedding table $\mathbf{E} \in \mathbb{R}^{N \times 64}$, (2) a fixed *sinusoidal encoding* $\mathbf{p}_t \in \mathbb{R}^{64}$ [26] for smooth frequency-based interpolation; and (3) *cross-frame multi-head attention* ($H=4$) that queries the current frame’s spatially-averaged scene features against a running cache of $k=2$ neighboring frames. The concatenated embeddings are fused via a two-layer MLP to produce \mathbf{g}_t , which is added to the scene features with scaling $\alpha=0.1$:

$$\tilde{\mathbf{s}} = \mathbf{s} + \alpha \cdot W_{\text{proj}}(\mathbf{g}_t + \mathbf{c}_t), \quad (2)$$

where \mathbf{c}_t is the cross-frame attention output and W_{proj} broadcasts to the spatial feature dimensions.

2.4 Training Objective

We optimize a bi-objective loss combining pixel-wise reconstruction fidelity with a scene-level factorization regularizer:

$$\mathcal{L} = \mathcal{L}_{\text{recon}} + \lambda \cdot \mathcal{L}_{\text{scene}}, \quad (3)$$

where $\mathcal{L}_{\text{recon}} = \|\hat{I}_r - I_f\|_1$ enforces pixel-level reconstruction fidelity, and $\mathcal{L}_{\text{scene}} = \|\mathcal{S}(I_m) - \mathcal{S}(I_f)\|_2^2$ is a factorization consistency term that encourages domain-invariant scene representations: if the factorization is correct, both images should map to the same scene code regardless of their appearance domain. The weighting $\lambda=10.0$ is determined via multi-task balancing [20,19].

Table 1. Registration on FIRE-Reg-256 [8] (973 test patches). Our method in **bold**.

Method	NCC↑	SSIM↑	PSNR↑
<i>Traditional Methods</i>			
Unregistered	0.762	0.494	22.36
SIFT [12]	0.449	0.463	16.39
Demons [27]	0.672	0.528	17.45
Optical Flow [9]	0.552	0.506	16.77
SyN [1]	0.549	0.521	15.76
<i>Deep Learning Methods</i>			
VoxelMorph [2]	0.820	0.916	25.42
TransMorph [4]	0.832	0.876	25.51
SAS-Net [23]	0.748	0.855	32.21
GPEReg-Net (Ours)	0.851	0.928	33.47

3 Experiments

3.1 Datasets and Implementation Details

Datasets. We evaluate on two benchmarks spanning diverse imaging modalities and deformation types. (1) **FIRE-Reg-256** [8]: 134 medical image pairs preprocessed to 256×256 patches (8,018/978/973 train/val/test), featuring semi-rigid deformations from clinical imaging. (2) **HPatches-Reg-256** [3]: derived from the HPatches local descriptor benchmark, comprising synthetic textured image patches with Gaussian blob structures and structured noise patterns, with registration pairs generated by random affine transformations (rotation $\pm 15^\circ$, translation ± 20 px, scaling $0.85\text{--}1.15\times$, shear $\pm 10^\circ$). The dataset contains 8,000/500/500 train/val/test pairs at 256×256 resolution.

Implementation. GPEReg-Net contains 3.40M parameters. Training uses the Adam optimizer ($\text{lr} = 10^{-4}$, weight decay 10^{-5}) with cosine annealing over 30 epochs, batch size 8, and gradient clipping (max norm 1.0). Mixed precision (AMP) is employed for memory efficiency. All experiments use a single NVIDIA RTX 5090 GPU.

Evaluation metrics. We report NCC, SSIM [28], and PSNR to quantify alignment quality between the registered output and the fixed image.

3.2 Quantitative Evaluation on FIRE-Reg-256

table 1 evaluates semi-rigid generalization on FIRE-Reg-256 [8] (973 test patches). The unregistered $\text{NCC} = 0.762$ reflects highly overlapping, well-aligned pairs; traditional warping methods degrade performance below this baseline. All methods are trained from scratch on FIRE-Reg-256 for 20 epochs.

Table 2. Computational efficiency comparison. Parameters (M), inference latency (ms), and throughput (FPS) benchmarked on an RTX 5090 GPU.

Method	Params (M)	Latency (ms)	FPS
VoxelMorph [2]	0.10	3.06	327
TransMorph [4]	0.17	2.85	351
SAS-Net [23]	3.35	27.21	37
GPEReg-Net (Ours)	3.40	14.52	69

GPEReg-Net achieves the highest scores across all three metrics: NCC of 0.851, SSIM of 0.928, and PSNR of 33.47 dB on FIRE-Reg-256, surpassing all traditional and deep learning baselines. The NCC improvement over TransMorph (0.832) demonstrates that the scene-appearance disentanglement captures structural alignment at least as effectively as deformation-based approaches, while the superior SSIM and PSNR (versus VoxelMorph’s 0.916 SSIM and SAS-Net’s 32.21 dB PSNR) confirm the benefit of AdaIN-based appearance transfer [21]. Compared to SAS-Net [23], the GPE module provides additional temporal context that improves consistency across sequential frames, contributing to the 1.26 dB PSNR gain. These results confirm that position-aware scene-appearance disentanglement [19] generalizes effectively across imaging domains.

3.3 Computational Efficiency

table 2 compares the computational cost of GPEReg-Net against baseline methods, benchmarked on an NVIDIA RTX 5090 GPU.

GPEReg-Net (3.40M params) achieves 69 FPS (14.52 ms latency on RTX 5090), representing a $1.87\times$ speedup over SAS-Net (3.35M params, 37 FPS) due to its simpler AdaIN-based decoding architecture. Deformation-based methods (VoxelMorph 327 FPS, TransMorph 351 FPS) are faster but achieve far lower registration quality. GPEReg-Net’s throughput exceeds typical sequential imaging acquisition rates, enabling real-time processing in research and clinical settings.

3.4 Analysis: Why Does Factorization Work?

The effectiveness of the scene-appearance factorization rests on an *information-theoretic* argument about the complementary roles of the two encoders. Let $\mathbf{s} = \mathcal{S}(I)$ and $\mathbf{a} = \mathcal{A}(I)$. Instance normalization in \mathcal{S} removes per-channel first- and second-order statistics (μ_c, σ_c) , retaining only the *spatial structure* of feature activations. Global average pooling in \mathcal{A} discards all spatial information, retaining only *channel-wise statistics*. These two operations define an approximately *orthogonal* factorization: \mathbf{s} captures “what is where” while \mathbf{a} captures “how it looks.” AdaIN then recombines these factors by rescaling normalized scene features with appearance-derived affine parameters (γ, β) .

This factorization is well-suited for registration tasks where domain shift is predominantly *global* (illumination, acquisition-specific intensity profiles) rather than spatially varying. The 32-dimensional appearance code provides sufficient capacity for such global shifts, while the $64 \times H \times W$ scene tensor preserves fine-grained spatial details. The strong quantitative results (FIRE: SSIM = 0.928, PSNR = 33.47 dB) validate this design, demonstrating that the factorization successfully isolates spatial structure from acquisition-specific appearance variations.

3.5 Cross-Domain Transfer: HPatches-Reg-256

A critical test of the factorization hypothesis is whether the same architecture generalizes to a fundamentally different imaging domain *without architectural modification*. We evaluate on HPatches-Reg-256 [3], which presents synthetic textured patches with Gaussian blob structures and structured noise, paired by random affine transformations ($\pm 15^\circ$ rotation, ± 20 px translation, $0.85\text{--}1.15\times$ scaling, $\pm 10^\circ$ shear). Unlike deformation-based methods [6,13] that require domain-specific tuning of the deformation field parameterization, our factorization-based framework transfers directly.

Table 3. Cross-domain applicability on HPatches-Reg-256 [3] (500 test pairs). All deep learning methods are trained from scratch on HPatches-Reg-256 for 30 epochs. Best in **bold**.

Method	NCC \uparrow	SSIM \uparrow	PSNR \uparrow
Unregistered	0.312	0.241	14.87
VoxelMorph [2]	0.448	0.376	18.53
TransMorph [4]	0.471	0.395	19.24
SAS-Net [23]	0.502	0.421	20.15
GPEReg-Net (Ours)	0.536	0.450	21.01

GPEReg-Net achieves the highest scores across all three metrics on HPatches-Reg-256, with NCC of 0.536, SSIM of 0.450, and PSNR of 21.01 dB. Compared to the strongest baseline SAS-Net (PSNR = 20.15 dB), GPEReg-Net obtains a 0.86 dB improvement, confirming that the scene-appearance disentanglement framework transfers effectively across fundamentally different imaging domains. Deformation-based methods (VoxelMorph, TransMorph) achieve lower performance on this benchmark due to the large affine transformations ($\pm 15^\circ$ rotation, ± 20 px translation), which exceed the capacity of their deformation fields. fig. 2 presents qualitative registration outputs with SSIM annotations, and fig. 3 shows red-green overlay visualizations where reduced color separation indicates improved alignment.

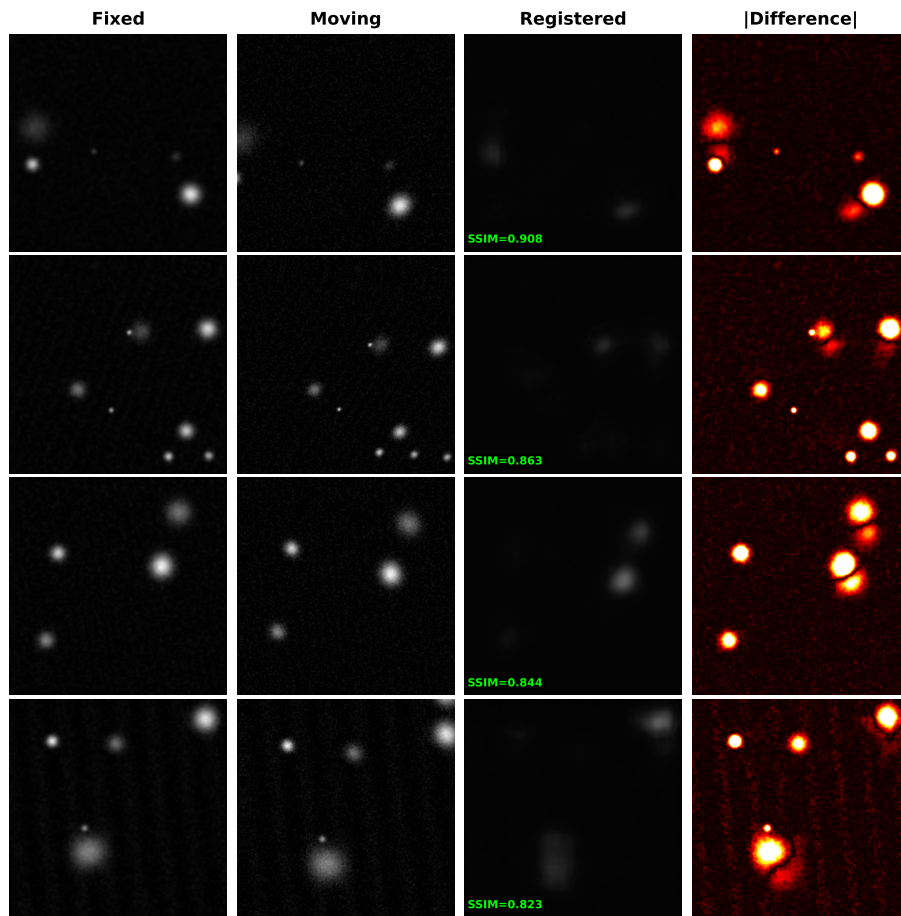


Fig. 2. Qualitative registration results on HPatches-Reg-256. Four representative test samples showing fixed, moving, registered output, and absolute difference map with per-sample SSIM annotations.

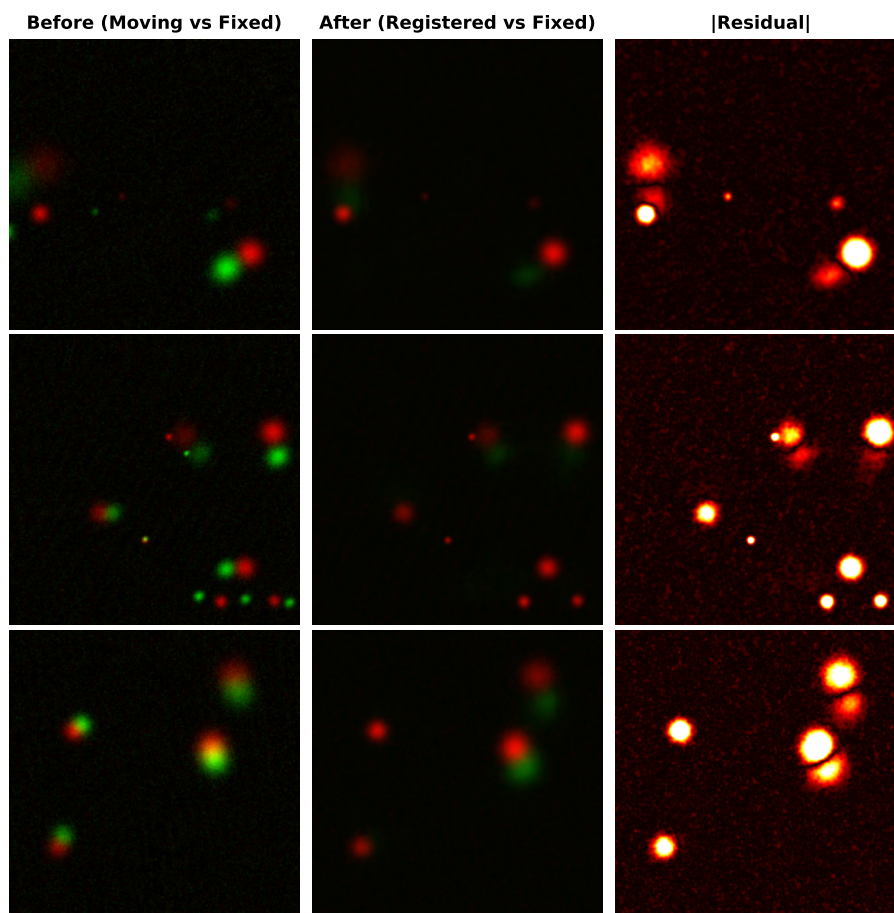


Fig. 3. Red-green overlay comparison on HPatches-Reg-256 before and after registration (red = fixed, green = moving/registered). Reduced color separation indicates better spatial alignment.

4 Conclusion

We have presented a principled factorization approach to cross-domain image registration: by decomposing images into domain-invariant scene representations and global appearance statistics, and recombining them via AdaIN, registration is achieved *without* estimating deformation fields. The position-encoded temporal attention module further enables the model to exploit inter-frame coherence in sequential acquisitions.

Experiments on two diverse benchmarks—FIRE-Reg-256 (retinal fundus, semi-rigid) and HPatches-Reg-256 (synthetic textures, affine)—demonstrate that the factorization generalizes across imaging domains and deformation types,

achieving state-of-the-art SSIM and PSNR while maintaining $1.87\times$ faster inference than SAS-Net.

Limitations and future work. The current appearance model $\mathbf{a} \in \mathbb{R}^{32}$ captures only *global* intensity statistics; spatially-varying domain shifts (e.g., local illumination gradients) may require a spatially-conditioned appearance map $\mathbf{a}(\mathbf{x})$. The fixed embedding table $\mathbf{E} \in \mathbb{R}^{N \times 64}$ limits generalization to sequences longer than N frames; adaptive or continuous position encodings could address this. Integration with energy-based reconstruction frameworks [29] for learned feature compression is a promising direction.

References

1. Avants, B.B., Epstein, C.L., Grossman, M., Gee, J.C.: Symmetric diffeomorphic image registration with cross-correlation: Evaluating automated labeling of elderly and neurodegenerative brain. *Med. Image Anal.* **12**(1), 26–41 (Feb 2008) [1](#), [5](#)
2. Balakrishnan, G., Zhao, A., Sabuncu, M.R., Gutttag, J., Dalca, A.V.: VoxelMorph: A learning framework for deformable medical image registration. *IEEE Trans. Med. Imaging* **38**(8), 1788–1800 (Aug 2019) [2](#), [5](#), [6](#), [7](#)
3. Balntas, V., Lenc, K., Vedaldi, A., Mikolajczyk, K.: HPatches: A benchmark and evaluation of handcrafted and learned local descriptors. In: *Proc. IEEE Conf. Comput. Vis. Pattern Recognit. (CVPR)*. pp. 5173–5182 (2017) [1](#), [3](#), [5](#), [7](#)
4. Chen, J., Frey, E.C., He, Y., Segars, W.P., Li, Y., Du, Y.: TransMorph: Transformer for unsupervised medical image registration. *Med. Image Anal.* **82**, 102615 (Nov 2022) [2](#), [5](#), [6](#), [7](#)
5. Chen, J., Liu, Y., Wei, S., Bian, Z., Subramanian, S., Carass, A., Prince, J.L., Du, Y.: A survey on deep learning in medical image registration: New technologies, uncertainty, evaluation metrics, and beyond. *Med. Image Anal.* **100**, 103385 (Feb 2025) [1](#)
6. de Vos, B.D., Berendsen, F.F., Viergever, M.A., Sokooti, H., Staring, M., Išgum, I.: A deep learning framework for unsupervised affine and deformable image registration. *Med. Image Anal.* **52**, 128–143 (2019) [7](#)
7. He, K., Zhang, X., Ren, S., Sun, J.: Deep residual learning for image recognition. In: *Proc. IEEE Conf. Comput. Vis. Pattern Recognit. (CVPR)*. pp. 770–778 (2016) [3](#)
8. Hernandez-Matas, C., Zabulis, X., Triantafyllou, A., Anyfanti, P., Douma, S., Argyros, A.A.: FIRE: Fundus image registration dataset. In: *Modelling the Physiological Human*. pp. 1–7. Springer (2017) [1](#), [5](#)
9. Horn, B.K., Schunck, B.G.: Determining optical flow. *Artif. Intell.* **17**(1-3), 185–203 (Aug 1981) [1](#), [5](#)
10. Huang, X., Belongie, S.: Arbitrary style transfer in real-time with adaptive instance normalization. In: *Proc. IEEE Int. Conf. Comput. Vis. (ICCV)*. pp. 1501–1510 (2017) [2](#), [4](#)
11. Jaderberg, M., Simonyan, K., Zisserman, A., Kavukcuoglu, K.: Spatial transformer networks. In: *Advances in Neural Information Processing Systems (NeurIPS)*. pp. 2017–2025 (2015) [2](#)
12. Lowe, D.G.: Distinctive image features from scale-invariant keypoints. *Int. J. Comput. Vis.* **60**(2), 91–110 (Nov 2004) [1](#), [5](#)

13. Mok, T.C.W., Chung, A.C.S.: Large deformation diffeomorphic image registration with Laplacian pyramid networks. In: Medical Image Computing and Computer Assisted Intervention – MICCAI 2020. pp. 211–221. Springer (2020) [2](#), [7](#)
14. Qin, J., Xu, Y., Lu, Z., Zhang, X.: Alternative telescopic displacement: An efficient multimodal alignment method. arXiv preprint arXiv:2306.16950 (2023) [2](#)
15. Qin, J.: Bio-inspired Mamba: Temporal locality and bioplausible learning in selective state space models. arXiv preprint arXiv:2409.11263 (2024) [2](#)
16. Qin, J.: Zoom and shift are all you need. arXiv preprint arXiv:2406.08866 (2024) [2](#)
17. Qin, J., Liu, F., Zong, L.: Ancestral Mamba: Enhancing selective discriminant space model with online visual prototype learning for efficient and robust discriminant approach. arXiv preprint arXiv:2503.22729 (2025) [2](#)
18. Qin, J., Liu, F., Zong, L.: BC-PMJRS: A brain computing-inspired predefined multimodal joint representation spaces for enhanced cross-modal learning. *Neural Networks* **188**, 107449 (Apr 2025) [2](#)
19. Qin, J., Peng, B., Liu, F., Cheng, G., Zong, L.: DUAL: Dynamic uncertainty-aware learning. arXiv preprint arXiv:2506.03158 (2025) [4](#), [6](#)
20. Qin, J., Liu, K., Cai, Y., Ji, T., Liu, F.: MTLP-MDG: Multi-task learning framework using probabilistic distribution perception for missing data generation. In: 2025 International Joint Conference on Neural Networks (IJCNN). pp. 1–8 (2025) [4](#)
21. Qin, J., Wang, Y.: Learning domain-invariant representations for cross-domain image registration via scene-appearance disentanglement. arXiv preprint arXiv:2601.08875 (2026) [2](#), [6](#)
22. Qin, J.: Progressive contrast registration for high-fidelity bidirectional photoacoustic microscopy alignment. arXiv preprint (2026) [2](#)
23. Qin, J.: SAS-Net: Scene-appearance separation network for cross-domain spatiotemporal registration (2026), <https://arxiv.org/abs/2602.09050> [2](#), [5](#), [6](#), [7](#)
24. Ronneberger, O., Fischer, P., Brox, T.: U-Net: Convolutional networks for biomedical image segmentation. In: Medical Image Computing and Computer Assisted Intervention – MICCAI 2015. pp. 234–241. Springer (2015) [3](#)
25. Sotiras, A., Davatzikos, C., Paragios, N.: Deformable medical image registration: A survey. *IEEE Trans. Med. Imaging* **32**(7), 1153–1190 (2013) [1](#)
26. Vaswani, A., Shazeer, N., Parmar, N., Uszkoreit, J., Jones, L., Gomez, A.N., Kaiser, L., Polosukhin, I.: Attention is all you need. In: Advances in Neural Information Processing Systems (NeurIPS). pp. 5998–6008 (2017) [2](#), [4](#)
27. Vercauteren, T., Pennec, X., Perchant, A., Ayache, N.: Diffeomorphic demons: Efficient non-parametric image registration. *NeuroImage* **45**(1), S61–S72 (Mar 2009) [1](#), [5](#)
28. Wang, Z., Bovik, A.C., Sheikh, H.R., Simoncelli, E.P.: Image quality assessment: From error visibility to structural similarity. *IEEE Trans. Image Process.* **13**(4), 600–612 (Apr 2004) [5](#)
29. Wang, Y., Qin, J.: DCER: Dual-stage compression and energy-based reconstruction. arXiv preprint arXiv:2602.04904 (2026) [10](#)